







## RESEARCH LETTER

# Integration of DNA–RNA-triplex-based regulation of transcription into molecular logic gates

Graziano Rilievo<sup>1</sup> , Alessandro Cecconello<sup>1</sup> , Nima Fouladi Gharehshiran<sup>1</sup> ,  
 Massimiliano Magro<sup>1</sup> , Friedrich C. Simmel<sup>2</sup>  and Fabio Vianello<sup>1</sup> 

<sup>1</sup> Department of Comparative Biomedicine and Food Science, University of Padova, Legnaro, Italy

<sup>2</sup> Physik Department, Technische Universität München, Garching bei München, Germany

## Correspondence

A. Cecconello, Department of Comparative Biomedicine and Food Science, University of Padova, viale dell'università 16, 35020 Legnaro (PD), Italy  
 Tel: +39 (0)49 8272916  
 E-mail: [alessandro.cecconello@unipd.it](mailto:alessandro.cecconello@unipd.it)

(Received 28 June 2023, revised 7 August 2023, accepted 8 August 2023, available online 31 August 2023)

doi:10.1002/1873-3468.14721

Edited by Michael Brunner

**In recent years, increasing numbers of noncoding RNA molecules were identified as possible components of endogenous DNA–RNA hybrid triplexes involved in gene regulation. Triplexes are potentially involved in complex molecular signaling networks that, if understood, would allow the engineering of biological computing components. Here, by making use of the enhancing and inhibiting effects of such triplexes, we demonstrate *in vitro* the construction of triplex-based molecular gates: ‘exclusive OR’ (XOR), ‘exclusive NOT-OR’ (XNOR), and a threshold gate, via transcription of a fluorogenic RNA aptamer. Precise modulation was displayed by the biomolecular-integrated systems over a wide interval of transcriptional outputs, ranging from drastic inhibition to significant enhancement. The present contribution represents a first example of molecular gates developed using DNA–RNA triplex nanostructures.**

**Keywords:** aptamer; *Escherichia coli*; fluorescence; promoter; synthetic biology;  $\sigma$ 70

In the toolbox of synthetic biology, the formation of alternative, non-duplex nucleic acid structures represents a valuable approach for the control of biochemical processes [1–3]. This is due to a number of reasons, including their involvement with biological targets such as gene promoters and endonuclease restriction sites [4,5], their tunability using specific stabilizing agents [6], and their compatibility with other natural or artificial single- and double-stranded nucleic acid structures [7,8]. In addition, non-canonical nucleic acid structures seem to play a role in cellular differentiation and cancer development via the regulation of gene expression [9]. These biological mechanisms can often be represented as gating mechanisms where molecular signals, among many stimuli,

interact with an ‘operator’ that interprets the signals as inputs, generating an output similarly to a gate [10], thereby implementing molecular computation. Among a number of nucleic acid supramolecular architectures, hybrid triplex structures comprise a duplex DNA and a single-strand RNA that interacts with a homopurine sequence (A, G) of the duplex, either in a parallel or antiparallel geometry. Figure 1A shows schematically the two main pyrimidine (C–G–C, T–A–U) and purine motifs (C–G–G, T–A–A) of hybrid DNA–DNA–RNA triplexes. These structures are stabilized by hydrogen bonds called Hoogsteen interactions [11], and they were proposed to play a role in gene regulation by competition with DNA-binding proteins [12].

## Abbreviations

DFHBI-1T, ((Z)-4-(3,5-difluoro-4-hydroxybenzylidene)-2-methyl-1-(2,2,2-trifluoroethyl)-1H-imidazol-5(4 H)-one); EMSA, electrophoretic mobility shift assay; lncRNA, long noncoding RNA; RNAP, RNA polymerase; rNTP, ribonucleoside triphosphate; TFO, triplex-forming oligonucleotide; TTS, triplex target site; TU, transcription unit; XNOR, exclusive NOT-OR; XOR, exclusive OR.

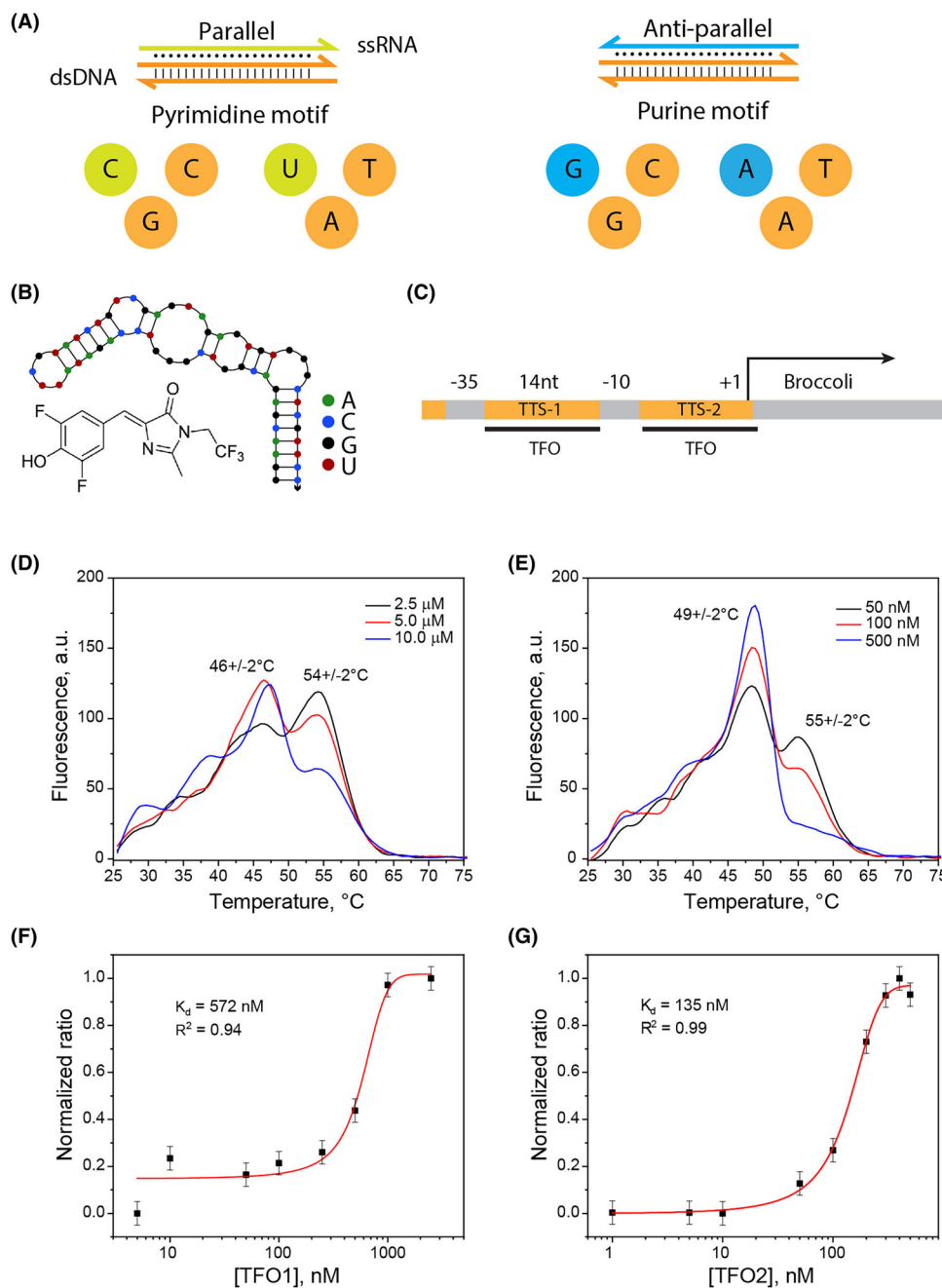


**Fig. 1.** (A) Schematic representation of the pyrimidine (left) and purine (right) motifs of the DNA–RNA triplex structures. Orange color identifies DNA, whereas green or blue color identifies pyrimidine- or purine-rich RNA, respectively. (B) Predicted structure of Broccoli aptamer and molecular structure of the fluorescent ligand DFHBI-1T. (C) Structure of the  $\sigma^{70}$  bacterial promoter. Triplex target sites TTS-1 and TTS-2 are indicated by orange portions, whereas the respective RNA TFOs are marked as black lines. –35, 14 nt, –10 and +1 indicate: the conserved sequence centered at 35 nucleotides upstream of the transcription initiation nucleotide, the 14 nucleotide nonconserved region, the conserved sequence centered at 10 nucleotides upstream of the transcription initiation nucleotide, and the transcription initiation nucleotide, respectively. (D, E) Melting curves showing thiazole green emission at 520 nm in a solution containing 100 nM double-strand TTS incubated with TFO1 (D) or TFO2 (E). Errors associated with the melting temperature were estimated from at least eight independent melting experiments. (F, G) Analysis of the TFO1-TTS or TFO2-TTS triplex melting curves, respectively, where the ratio of the triplex/duplex peaks shown in D and E is plotted against the respective TFO concentration. Error bars represent the standard deviation of three independent experiments. TTS and TFOs individual curves are reported in Figures S1 and S2.

Recently, a family of RNAs termed long noncoding RNAs (lncRNAs) has been associated with gene regulation in eukaryotes, where the involvement of RNA–DNA triplexes has been suggested [13,14]. The discovery that DNA/RNA nanostructures play a more fundamental role in organisms than previously thought has blurred the boundaries between applications in nanomaterials and in the biological sciences [1,15,16]. The recent introduction of fluorogenic RNA aptamers, along with the commercial availability of affordable custom-sequence oligonucleotides, provided the field with powerful tools for the study of such nucleic acid structures [14,17–20]. Specifically, *in vitro* polymerization of fluorogenic RNA aptamers allows the detection of transcriptional activity by fluorescence emission changes, which are associated with the increasing concentration of the RNA–ligand complex [21–24]. This method allows the direct measuring of transcription rates along with transcript visualization and microscopic localization, avoiding additional staining and therefore preventing the introduction of external biases.

The potential of RNA triplex-forming oligonucleotides (TFOs) as molecular tools for the up- or down-regulation of transcription was first highlighted in a recent publication from our group [25]. Briefly, the formation of the triplex complex affected the rate of transcription depending on (a) triplex target site (TTS) distance from position +1 (i.e., start of the transcript), (b) the position of the TTS in the sense strand or the template strand, and (c) triplex motif. Here, the optimization of the different parameters affecting triplex yield, the fine-tuning of polymerization rates, along with previously uncovered molecular details of the TFOs and transcription units (TUs) are described and discussed. Most importantly, we demonstrated the feasibility of using triplexes as biomolecular transducers of logic gate mechanisms and therefore their possible future application for the construction of biocomputing networks in cells [10,26]. Specifically, we show representative triplex-based designs showing logic gate output behavior (XOR and XNOR) and the molecular implementation of a threshold gate [27,28]. Overall, the present contribution gives proof of the integration of enhancing and inhibiting triplex effectors, resulting in an extended range of transcription modulation that far exceeds previous reports and paves the way for its use in a transcription–translation system.

## Materials and methods

### Reagents

All nucleic acid sequences are listed in Table S1 and were purchased from IDT (Integrated DNA Technologies, Inc.

Coralville, Iowa, USA). Stock solutions were prepared in water and stored at  $-20^{\circ}\text{C}$ . The ribonucleotide mix (rNTPs) and the *Escherichia coli* RNA polymerase (RNAP) holoenzyme were purchased from New England BioLabs Inc. (Ipswich, MA, USA) and stored at  $-20^{\circ}\text{C}$ . The buffers used for the experimental parts were Tris–HCl (J.T. Baker, Avantor-VWR, PA, USA), MES (Sigma-Aldrich–Merck, Darmstadt, Germany), and TBE buffer (Millipore, Millipore-Merck, Darmstadt, Germany). Concentrated HCl was purchased from Sigma-Aldrich, and NaOH was purchased from J.T. Baker. KCl,  $\text{MgCl}_2$ , dithiothreitol (DTT), Triton X-100, acrylamide/bisacrylamide 19 : 1 solution, ammonium persulfate (APS), N,N,N',N'-tetramethylethylenediamine (TEMED), sodium dodecyl sulfate (SDS), and bromophenol blue were purchased from Sigma-Aldrich. Nucleic acid stains oxazole gold and thiazole green were purchased from Biotium Inc., Fremont, CA, USA. DFHBI-1T ((Z)-4-(3,5-difluoro-4-hydroxybenzylidene)-2-methyl-1-(2,2,2-trifluoroethyl)-1H-imidazol-5(4 H)-one) was purchased from Lucerna Inc. All solutions were prepared using ultrapure water from a Genie Direct-Pure water device (RephiLe Bioscience Ltd., Shanghai, China), with a resistivity of at least 18.0 M $\Omega$ -cm.

### Instrumentation

Double-strand annealing procedure was performed with a Mastercycler Nexus-GX (Eppendorf Inc., Hamburg, Germany). Time-dependent fluorescence measurements were performed using a Clariostar (BMG LABTECH, Ortenberg, Baden-Wuerttemberg, Germany) with 384-wells Corning Inc. (New York, NY, USA) plates, except for time-dependent fluorescence measurements regarding the threshold gate, where a VICTOR X4 2030 Multilabel Reader (Perkin Elmer, Waltham, MA, USA) with 485/535 nm excitation/emission filters was used along with Lumox 384 multiwell plates (Sarstedt, Nümbrecht, Germany). Melting temperature experiments were conducted using a Stratagene Mx3000P (Agilent Technologies, Santa Clara, CA, USA) and samples were placed in tubes with optically clear caps (Thermo-Fisher Scientific Inc., Waltham, MA, USA). Electrophoresis runs were conducted in a Mini-PROTEAN Tetra System electrophoresis chamber (BIO-RAD, Hercules, California, USA), connected to a PowerEase Touch 350 W power supply (Invitrogen-Thermo Fisher, Waltham, MA USA). Electrophoresis gel fluorescence images were acquired with an iBright1500 imaging system (Invitrogen-Thermo Fisher Scientific168 Third Avenue Waltham, MA, USA).

Data analysis software used to produce all the statistical and graphical analyses was ORIGINPRO 2018B (OriginLab Corp., Northampton, MA, USA).

### Sample preparation

All double-strand DNA was prepared in the Mastercycler by annealing 10  $\mu\text{M}$  of the complementary strands in

50 mM NaCl, with a temperature ramp from 95 to 25 °C. The stock solutions were stored at –20 °C.

Samples for the RNA-polymerization experiments, the temperature-dependent denaturation experiments, and the electrophoretic mobility shift assay (EMSA) were prepared in a modified version of the RNA-polymerization buffer recommended by New England BioLabs. The buffer composition for this work was: 40 mM Tris–HCl, 150 mM NaCl, 30 mM MgCl<sub>2</sub>, 1 mM DTT, and 0.01% Triton X-100, at pH 6.9. For the pH optimization, Tris–HCl buffer was replaced with MES 40 mM and the different pH values were obtained with small volumes of concentrated NaOH or HCl. EMSA experiments were carried out in 12% acrylamide/bis-acrylamide 19:1 gels, prepared in 1X TBE buffer at pH 6.9, containing 10 mM MgCl<sub>2</sub>, 1.25 mg/mL APS, and 0.05% TEMED. The electrophoresis run was conducted in ice at 75 V for 2 hours. The gel was then stained for 10 minutes under gentle agitation in a freshly made staining solution containing oxazole gold IX. After that, the gel band emission was acquired using UV excitation.

### Triplex denaturation analysis

Temperature-dependent denaturation was performed using 100 nM TTS in the presence of different TFO1 or TFO2 concentrations, in the modified RNAP reaction buffer. After 30-min incubation at 4 °C, 10 µL of the mixture was transferred in a tube containing 8 µL of water and 2 µL thiazole green solution. The analysis was performed in a Stratagene Mx3000P that measured fluorescence emission in a temperature ramp. Denaturation curves of individual RNA strands and the dsDNA only are reported in Figures S1 and S2.

### RNA-polymerization rate analysis

The polymerization rates were assessed using 16 U·mL<sup>–1</sup> of RNAP, 160 µM DFHBI-1T, in the absence of TFOs (optimization experiments), in the presence of one or two TFOs (XOR and XNOR gates), in the presence of two TFOs (threshold gate), or the TFO was produced *in situ* (molecularly wired system). First, the polymerization rates of different samples containing 200 nM double-strand DNA transcription unit TU1 in the pH range 5.5–7.5 was evaluated. Similarly, double-strand DNA template concentrations in the range 30–600 nM were used to establish their effect on transcription. Lastly, the rNTP concentration was evaluated. In that case, rNTP concentrations ranging from 0.5 to 4.0 mM were used in the RNA-polymerization reaction in the presence of 40 nM of the double-strand template. After this optimization step, all following experiments were conducted at pH 6.9, 200 nM template, and 4 mM ribonucleotide mix.

When RNA duplex formation was needed, the two strands were incubated in equimolar concentrations and allowed to anneal for 30 min. For the threshold gate, different ratios of TFO1 (input, I) and TFO2 (threshold, Th) concentrations were tested in the presence of the double-strand template. Samples were prepared with a TFO1:TFO2 ratio ranging from 0.01:1 to 100:1 (individual oligonucleotide concentrations ranged from 1 nM to 10 µM), with a constant concentration of TU8 equal to 100 nM. The samples were incubated for 30 min at 4 °C in the modified RNAP reaction buffer at pH 6.9. After incubation, the polymerization reaction was started by adding 16 U·mL<sup>–1</sup> of RNAP and 4 mM rNTPs. Fluorescence emission due to fluorophore binding on the newly formed RNA aptamer was collected with Victor X4 plate reader. Measurements were conducted at 29 °C for 5 h, and the fluorescence data were fitted linearly in a time period of 120 minutes, once reached stability (typically 1 hour after the start of polymerization). Fluorescence rates, estimated as emission intensity changes over time, were computed and plotted with OriginPro software.

## Results

*Escherichia coli*  $\sigma^{70}$ -based engineered TUs comprising a promoter upstream of a transcription template for Broccoli fluorogenic aptamer were sequence-modified to contain targets (TTSs) for the triple-helical complex formation with an RNA oligo (all DNA and RNA sequences are reported in Table S1). Figure 1A depicts schematically the nucleobases of the most stable hybrid triplexes representing the all-purine or all-pyrimidine motifs [29,30]. These short RNA sequences, named triplex-forming oligonucleotides (TFOs), were tested for their effect on the transcription rate of engineered TUs. The transcription rates were estimated using the fluorescence emission changes associated with Broccoli aptamer-DFHBI-1T complex formation, and its accompanying quantum yield increase, during *in vitro* RNA polymerization. Figure 1B shows Broccoli ligand DFHBI-1T, and the aptamer predicted secondary structure ([nupack.org](http://nupack.org), Caltech), where the end stem was extended to increase the aptamer stability. Three different TTS designs could be placed within the unconserved regions of the  $\sigma^{70}$  promoter (Fig. 1C, see Table S1 for details regarding the sequence design). Specifically, these TUs, based upon *E. coli* general promoter architecture, comprised consensus sequences –35 and –10 and artificial TTSs introduced between these two sequences (TTS-1) or between –10 and the transcription starting nucleotide +1 (TTS-2). A third design included both TTSs in the same promoter and was termed TTS-3.



Triplex formation was assessed using melting curve analysis (Fig. 1D,E). In these experiments, we aimed at improving the current methods for triplex analysis affected by a general issue regarding melting temperature determination based on classical hyperchromicity experiments or fluorophore-modified oligonucleotides. We used nucleic acid fluorescent stain thiazole green (emission at 520 nm) as a reporter for triplex and duplex denaturation. The curves clearly show two peaks that were attributed to the denaturation event of the TFO1- or TFO2-TTS triplexes and the duplex DNA, at corresponding melting temperatures  $46 \pm 2^\circ\text{C}$  or  $49 \pm 2^\circ\text{C}$  and  $55 \pm 2^\circ\text{C}$ , respectively (Fig. 1D,E, respectively). The results indicated that triplex separation occurred at lower temperatures in respect to the duplex, in accordance with the lower stability of the three-strand complex. It is worth noting that the current method of melting temperature determination using a common nucleic acid fluorescent stain allowed the successful discrimination between the denaturation peaks of duplexes and triplexes for both the TFO-TTS pairs [25]. Furthermore, melting curve analysis shown that a sigmoid fit of the normalized triplex melting temperatures in an interval of TFO concentrations, Fig. 1F,G, resulted in dissociation constants related to pyrimidine and purine motifs, equal to 572 and 135 nM, in agreement with previously reported values.

On these bases, an atlas of enhancing and inhibitory TTS-TFO combinations was designed, integrating their effects into more complex TUs (Fig. 2A). The left part of the panel shows the geometry of the TTSs within the TU, while the right part of the panel shows the triplex formation effect on the polymerization rate of Broccoli (red bars indicate the percentage of inhibition, while green bars indicate percentages of enhancement). The strongest inhibitory effect ( $\approx -90\%$ ) was shown by two purine motif TTSs, while the strongest enhancement was shown by two pyrimidine motif TTSs ( $\approx +200\%$ ) located in the same promoter. The authors believe that such TTS-TFO interactions can ideally be expanded beyond the building of an ON/OFF digital system and be used to obtain, for instance, continuous-value computing based on molecular mechanisms [31].

In the next step, we focused on optimizing the polymerization conditions, and thus, a set of experiments were conducted to test the system. First, a pH-dependent activity assessment, using transcription unit TU1, in a pH range between 5.5 and 7.5, showed that, in our experimental conditions, the pH optimum of the *E. coli* RNAP for Broccoli production is found at basic pH values [32], albeit still showing activity at slightly acidic conditions (Fig. 2B). Since, on the

one hand, acidic pH inhibits RNAP enzymatic catalysis but, on the other, a basic pH destabilizes the pyrimidine motif triplex, near-neutral pH was selected to be used for triplex formation, as a compromise between the pH optimum of the enzyme and a triplex-formation promoting pH.

Figure 2C shows the relative rates of transcription at 40 nM duplex DNA template in the presence of different concentrations of the ribonucleotide mix (from 0.5 to 4 mM) showing a linear dependence. For the RNA-polymerization protocol, we selected the highest concentration tested (i.e., 4 mM) to ensure a continuous presence of the ribonucleotides even for long-time experiments. This is particularly relevant since the polymerization rate should not be limited by ribonucleotide unavailability.

Lastly, the appropriate concentration of double-strand template was assessed. An interval of template concentrations, from 30 to 600 nM, was tested, showing the activity maximum at 200 nM (Fig. 2D). This optimum might be attributed to the sigma factor dilution effect, that is, at high template concentrations, the  $\sigma^{70}$  factor molecules are associated with the excess template, reducing the total number of active holoenzyme complexes (RNAP + sigma factor) and thus resulting in a lower transcription rate. We felt these optimization steps necessary to adapt the commercial holoenzyme to the triplex assay. This will allow others to replicate the experiments more effortlessly and to adjust the different parameters depending on the specific tests.

Since the structure of the TFO strongly affects the formation of the hybrid triplex, we investigated how the presence of 1, 2, or 3 tandem repeats of TFO domains comprised in one RNA strand affected transcription. The TFOs were produced *in situ* and were designed to target a promoter (TU2) in the same solution via a process called 'molecular wiring'. Figure 3, panels A–C, shows schemes of the molecular wiring of transcription units TU3, TU4, and TU5, where TU2 contains two TTSs (orange bars), generating inhibitory triplexes with TFOs (blue bars). In the first case, panel A, TU3 produces RNA containing one TFO domain, 1XTFO, while in the two following cases, TU4 and TU5 encode two and three TFO domains, 2XTFO or 3XTFO, respectively, separated by four nucleotides within the same filament (spacers represented by thin black lines), panels B and C. We hypothesized that once a triplex is formed within a tandem repeat, a local concentration of the TFO is generated thus stabilizing the complex. Assuming a negligible volume increase for the three TFOs, the local concentration of the triplex-forming RNA sequence doubles for 2XTFO and triples for 3XTFO, in respect to 1XTFO, due to

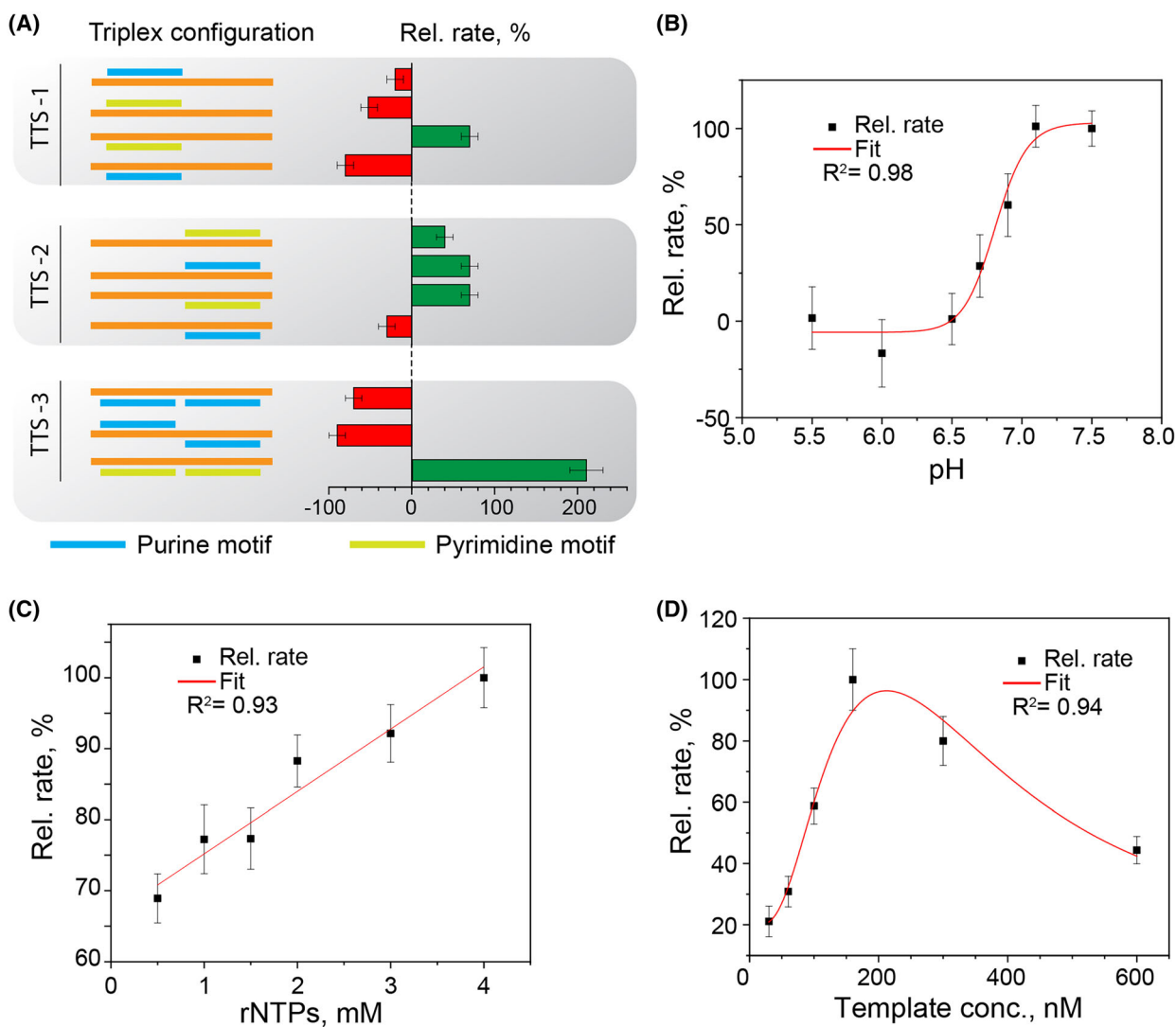


**Fig. 2.** (A) Schemes of the engineered artificial promoters (orange line) showing the different pyrimidine (green line) or purine (blue line) triplex geometries and the associated effects on the transcription rate represented as percentages of inhibition (red) or enhancement (green). Designs are grouped as containing one TTS upstream of  $-10$  (TTS-1), containing one TTS upstream of  $+1$  (TTS-2), or containing combinations of two TTSs (TTS-3). Left part: The geometry of the TTSs within the transcription unit; right part: Triplex formation effect on the polymerization rate of Broccoli (red bars indicate the percentage of inhibition, while green bars indicate percentages of enhancement). The strongest inhibitory effect ( $\approx -90\%$ ) was found for two purine motif TTSs, while the strongest enhancement was found for two pyrimidine motif TTSs ( $\approx +200\%$ ) located in the same promoter. (B) RNA-polymerization relative rates at different pH values. (C) RNA-polymerization relative rates at different ribonucleoside triphosphate (rNTP) concentrations. (D) RNA-polymerization relative rates in the presence of different Broccoli template concentrations. Error bars represent the standard deviation of three independent experiments.

the tandem repeats. In other words, for 1XTFO the local concentration equals its bulk concentration, while for 2XTFO and 3XTFO the local concentration must be higher than the bulk and dependent on the number of repeats. Panels on the right of each molecular wiring scheme show the respective Broccoli synthesis rates plotted against the increasing ratios of the wired TUs. The sigmoid fit clearly shows a shifting of the curve to the left toward lower ratios ( $2.1 > 0.7 > 0.3$ ) of the

TFO-encoding TU in respect to TU2 and thus supporting the stronger effect of the triplexes associated with higher local concentrations (additional experimental details are reported in the methods section).

To further demonstrate the applicability of the enhancing/inhibiting hybrid triplexes, logic gates XOR and XNOR were produced. Such gates can be easily interpreted as operators that give a positive signal (output = 1, high transcription rate) when the two

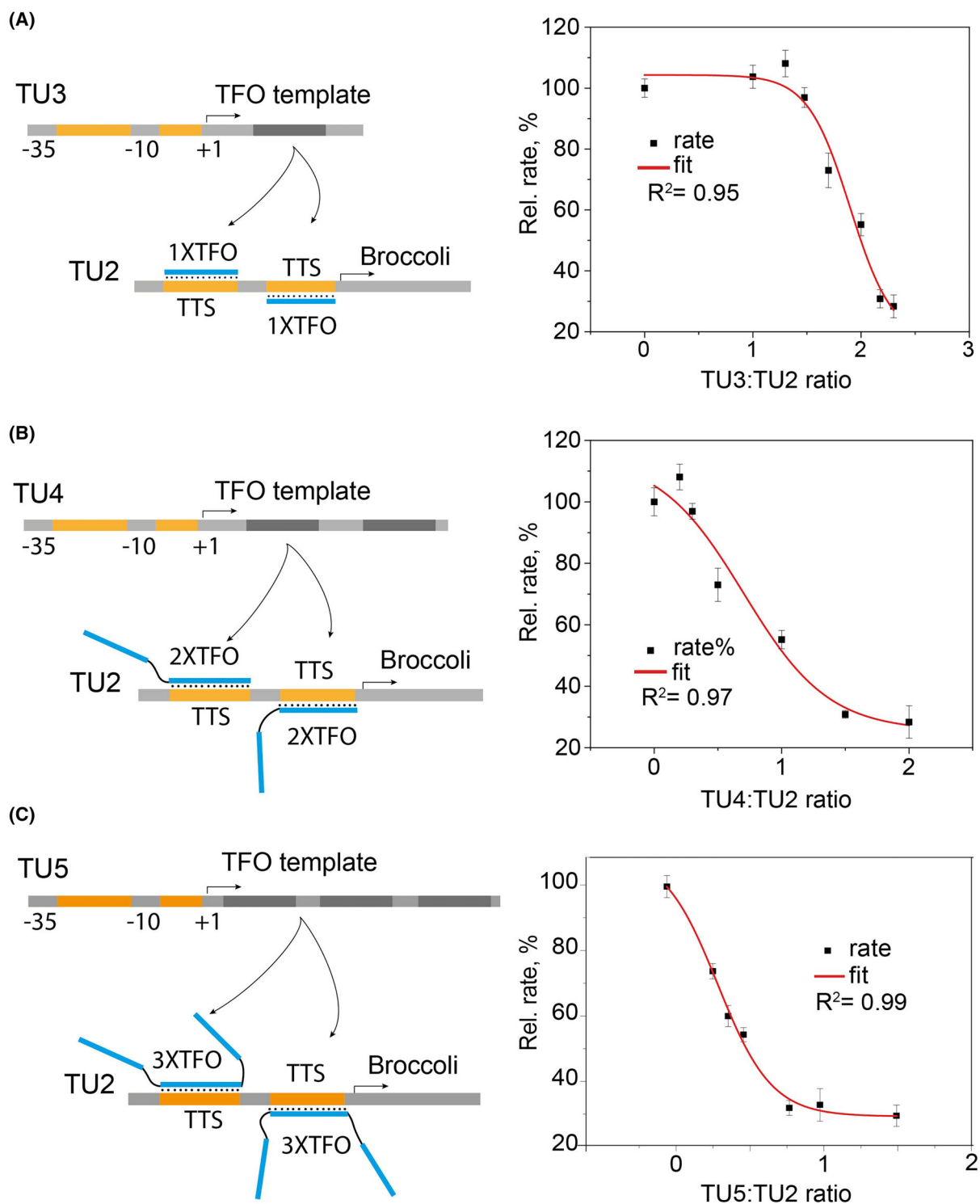


**Fig. 3.** Schemes on the left describe graphically the molecular wiring of transcription units TU2, TU3, TU4, and TU5, where TU2 contains the target sites (TTS, orange portions) for the *in vitro* polymerized TFOs (blue bars) containing only one duplex interacting portion, 1XTFO, panel A (50% inhibition at TU3/TU2 ratio = 2.1), containing two TFO tandem repeats, 2XTFO, panel B (50% inhibition at TU4/TU2 ratio = 0.7), or containing three TFO tandem repeats, 3XTFO, panel C (50% inhibition at TU5/TU2 ratio = 0.3). Plots on the right side show representative polymerization rates at different ratios or TFO-producing/reporter TUs. Errors bars depict standard deviations of the polymerization rate linear fittings. 50% inhibition ratios were obtained from three independent experiments.

inputs have different values (either one TFO is present but not both, XOR gate) or when the two inputs (TFOs) have the same value (both TFOs present or both TFOs absent, XNOR gate). Their molecular implementation is the following: Sequence-complementary TFO1 and TFO2 were used as inputs ( $I_1$  and  $I_2$ , respectively), the transcription unit (TU6 or TU7 for XOR or XNOR, respectively) represented the logic operator, while the transcription rate was used as output, and Broccoli fluorescence was used as readout. For the XOR gate, two enhancement triplexes were used, resulting in an enhancement effect when only one input was present (ssRNA TFO available to form a triplex) and unperturbed transcription when none or both were present (duplex RNA unavailable to form a triplex). Figure 4A shows the kinetics of Broccoli polymerization at four conditions: In the absence of both TFOs, in the presence of only one of the two TFOs, and in the presence of both TFOs, reflecting input combinations 0–0, 0–1, 1–0, and 1–1. The linear rate values and the truth tables are reported on the right of the respective kinetic plots, where an arbitrary threshold was set at 80% of the highest transcription rate and thus setting the 0 or 1 output values for the lower or higher rates, respectively. Schemes of the molecular duplex (orange bar) and TFOs (green and blue bars) generating triplexes are shown on the right of each truth table input combination. Similarly, Fig. 4B shows the molecular implementation of logic gate XNOR where complementary-sequence inhibitory TFOs were used. The presence of both TFOs or the absence of both resulted in transcription rates higher (output = 1) than an arbitrary threshold set at 60% of the highest rate, while the presence of either one of the inhibitory TFOs resulted in lower rates than the threshold (output = 0). The respective bar plot and truth table are reported on the right of the kinetics graph. As for the previous gate, DNA–RNA complex schematics are shown on the right of the truth table, following the same color scheme.

Following the approach used for the molecular logic gates, a triplex-mediated threshold gate was built. A threshold gate operates a signal transduction analogous to a neuron where inputs are first used to generate a sum and this value is then used to produce a positive output (sum higher than the threshold) or a zero output (sum lower than the threshold). In this case, two complementary-sequence TFOs were used to build triplexes with opposite effects (inhibiting or enhancing) that modulated the polymerization rate output from transcription unit TU8. The enhancing TFO represented the input and the inhibiting TFO represented the threshold. This allowed an inhibition/

enhancement polarized effect depending on the TFO with the higher concentration. The threshold gating effect resulted in the TU positively modulated when the input concentration was higher than the threshold and negatively modulated in the opposite case. Figure 4, panel C, shows a collection of rates recorded at different input/threshold ratios showing a zero output for ratios lower than 1 and a positive output at higher input/threshold ratios. On the right side of the panel, schemes of the DNA–RNA interactions at increasing input/threshold ratios are shown (bottom to top). Figure 4, panel D, shows an additional EMSA characterization of the threshold gate where the triplex-associated band, indicated by a green arrow, becomes more intense when input/threshold concentration ratios are farther from one, while the band disappears when the two RNAs are present at equimolar concentrations. This means that in the presence of an excess of either RNA strand, the triplex is stabilized (leftmost and rightmost lanes) whereas the equimolar concentrations of the two destabilizes the triplex shifting the equilibrium toward the more stable duplex RNA. Therefore, the here reported examples give proof of the feasibility of developing molecular gates using a triplex-operated transcription system.

## Discussion

Protein-based transcription factors have been extensively used in synthetic biology to modulate transcription processes and generate synthetic gene regulatory networks [10,26]. Conversely, although currently being an active object of research due to their potential involvement in the biological activity of lncRNAs [13,33], the transcription regulation effects of RNA–DNA triplexes are far from being fully understood. In fact, nowadays the research on lncRNAs produced an impressive number of computational tools and databases [34,35] that are constantly updated with the inflow of new experimental data. The *E. coli*  $\sigma^{70}$  promoter represents an ideal architecture for studying the effect of these hybrid triplexes on DNA-interacting proteins such as RNAP [7]. By engineering its nonconserved domains, formation of sequence-dependent triplexes with an external RNA strand was promoted. Moreover, we showed that such alterations did not prevent transcription that was in fact optimized for ribonucleotide concentration, duplex template concentration, and pH (Fig. 2). Triplex formation, and its associated effects on transcription, on the contrary, was strengthened when TFO tandem repeats were placed in the same RNA in a molecularly wired system, due to the increased TFO local concentration (Fig. 3).



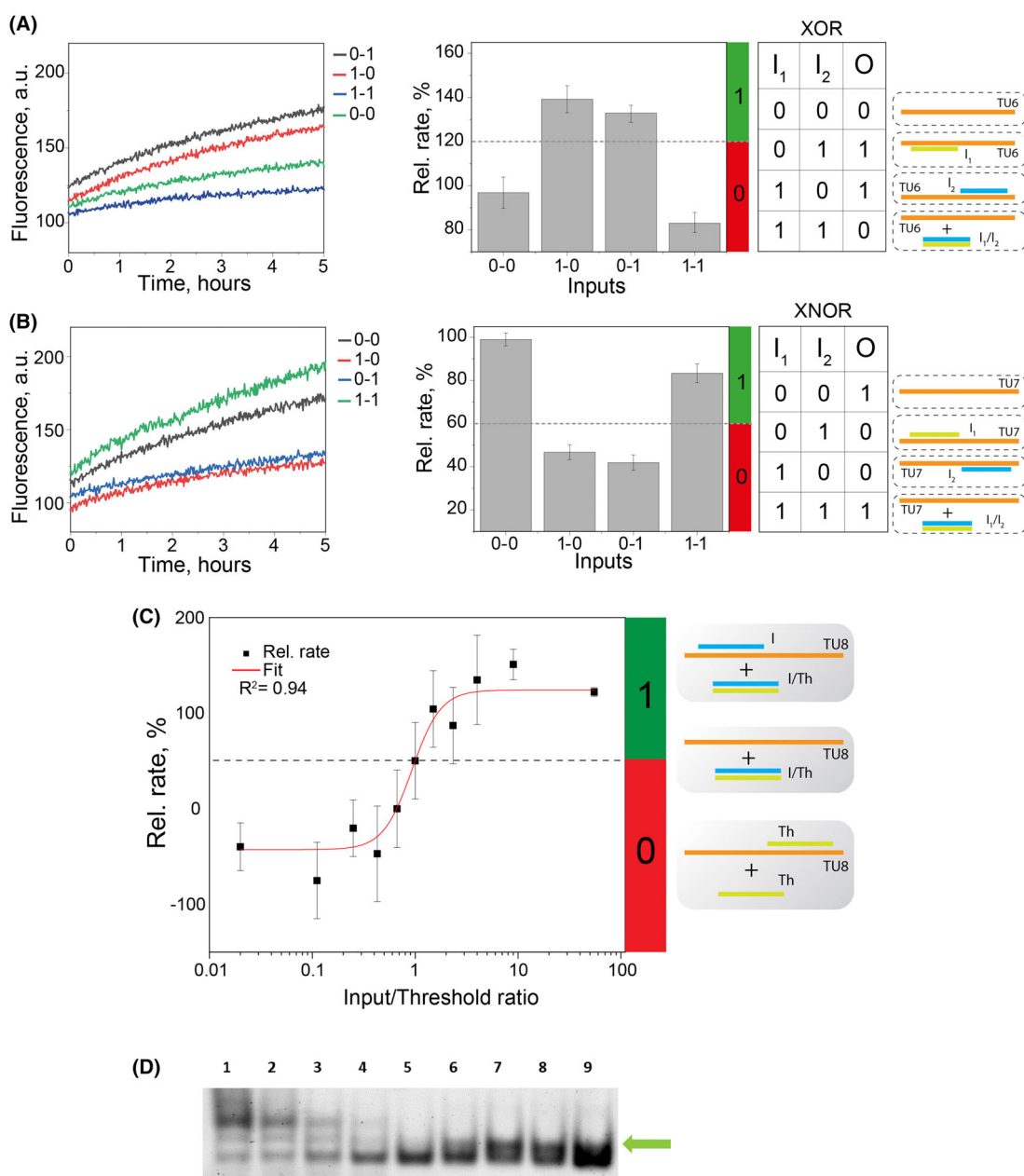


**Fig. 4.** Triplex-based molecular logic gates and a threshold gate. (A, B) Fluorescence signals of Broccoli *in vitro* synthesis from transcription units TU6 or TU7 incubated with TFOs  $I_1$  and  $I_2$  combinations representing inputs. The linear fluorescence-estimated polymerization rates are depicted in the bar plots on the right and the outputs followed a XOR gate or a XNOR gate depending on the promoter design. Each bar plot is accompanied by the corresponding logic gate truth table where schemes of the input/gate states are schematically depicted for each input combination. TFOs are represented as green and blue bars (pyrimidine and purine TFO, respectively), and the duplex DNA promoter acting as gating unit is shown as an orange bar. (C) Experimental results showing the implementation of a threshold gate using two TFOs as input ( $I$ ) and threshold ( $Th$ ), respectively, and the transcription unit TU8. The estimated linear polymerization rates were used as outputs and are plotted against the input/threshold concentration ratio. On the right, schemes of the DNA–RNA interactions are shown for the case limit at low  $I/Th$  ratios (bottom, output = 0), at ratio = 1 (middle, threshold), and at high ratios (top, output = 1). (D) Electrophoretic analysis of the input, threshold, and duplex DNA interactions demonstrating the formation of the transcription enhancing/inhibiting triplex structures associated with the band indicated by the green arrow (lanes 1 to 9: Input concentrations were 1nM to 10 $\mu$ M while threshold concentrations were 10 $\mu$ M to 1nM). The band disappears at input/threshold ratios close to 1 (lane 5). Error bars represent the standard deviation of three independent experiments.

Taking inspiration from pioneering works on DNA computing [36], a XOR gate, a XNOR gate, and a threshold gate were built, Fig. 4. Indeed, the outputs behaved according to the respective truth tables when enhancing (XOR) or inhibitory inputs were used (XNOR), while the threshold gate made use of both enhancing and inhibitory inputs. At low input concentrations, the output was zero (low, inhibited transcription of Broccoli) while when the input concentration was higher than the threshold (i.e., input/threshold, ratio > 1) the output was equal to 1 (i.e., high, enhanced Broccoli transcription), Fig. 4C. Noteworthy, these effects are dictated by sequence complementarity of the two TFOs, as demonstrated by the EMSA characterization, Fig. 4D, and can in principle be implemented in a molecularly wired system, as demonstrated here and elsewhere [25], thereby allowing for more complex networks (e.g., molecular oscillators, pulse generators, or bistable circuits).

The gates proposed in this contribution will set the ground for implementing multigated transcriptional activities using different fluorescent RNA aptamers (e.g., Corn, Spinach, or Mango) for the development of more complex computations [27,28]. *In vivo* monitoring of such systems is also foreseen; in this way, switchable triplex structures might be designed to turn ON or OFF different TUs depending on the TTS position and the TFO used. Finally, while the mechanism of the inhibitory effect had been previously investigated and attributed to a competition phenomenon [7,12], enhancement was only recently discovered and its mechanism has not been elucidated yet. Therefore, the authors believe that the potential involvement of triplex-mediated transcription regulation with biological processes of multicellular organisms such as cell differentiation, metabolism, and circadian rhythm [37,38] justifies promoting its further investigation. In addition, we suggest that the interplay between triplex stabilizing molecules (e.g., polyamines, nucleic acid intercalators, and positively charged peptides) and ssRNA might provide a universal way of gene regulation, which might also have mechanistic relevance at the root of several elusive diseases caused by abnormal transcription [39,40], as well as applications in artificial biological components [41].

## Acknowledgements

AC is supported by a Long-Term EMBO fellowship [ALTF 433–2018]; REACT EU–PON ‘Ricerca e Innovazione 2014–2020’; MM is supported by the grant ‘Giovani Ricercatori – Third call’ funded by the Department of Comparative Biomedicine and

Food Science, University of Padova; Italian Ministry of Education, University and Research (MIUR) ‘Centro di Eccellenza per la Salute degli Animali Acquatici – ECCE AQUA’.

## Author contributions

GR, AC, and NFG performed the experiments. AC designed the system. All authors analyzed, interpreted, and commented the experimental results. All authors wrote, revised, and edited the manuscript.

## Peer review

The peer review history for this article is available at <https://www.webofscience.com/api/gateway/wos/peer-review/10.1002/1873-3468.14721>.

## Data accessibility

The Supporting Information file contains all nucleic acid sequences used in this study (Table S1) and additional melting curves (Figures S1 and S2).

## References

- Hu Y, Cecconello A, Idili A, Ricci F and Willner I (2017) Triplex DNA nanostructures: from basic properties to applications. *Angew Chem Int Ed Engl* **56**, 15210–15233.
- Frank-Kamenetskii MD and Mirkin SM (1995) Triplex DNA structures. *Annu Rev Biochem* **64**, 65–95.
- Sun JS, Garestier T and Hélène C (1996) Oligonucleotide directed triple helix formation. *Curr Opin Struct Biol* **6**, 327–333.
- Hanvey JC, Shimizu M and Wells RD (1990) Site-specific inhibition of EcoRI restriction/modification enzymes by a DNA triple helix. *Nucleic Acids Res* **18**, 157–161.
- Postel EH, Flint SJ, Kessler DJ and Hogan ME (1991) Evidence that a triplex-forming oligodeoxyribonucleotide binds to the c-myc promoter in HeLa cells, thereby reducing c-myc mRNA levels. *Proc Natl Acad Sci USA* **88**, 8227–8231.
- Escudé C, François JC, Sun JS, Ott G, Sprinzl M, Garestier T and Hélène C (1993) Stability of triple helices containing RNA and DNA strands: experimental and molecular modeling studies. *Nucleic Acids Res* **21**, 5547–5553.
- Bervoets I and Charlier D (2019) Diversity, versatility and complexity of bacterial gene regulation mechanisms: opportunities and drawbacks for applications in synthetic biology. *FEMS Microbiol Rev* **43**, 304–339.

- 8 Ng C, Samanta A, Mandrup OA, Tsang E, Youssef S, Klausen LH, Dong M, Nijenhuis MAD and Gothelf KV (2023) Folding double-stranded DNA into designed shapes with triplex-forming oligonucleotides. *Adv Mater* e2302497. doi: [10.1002/adma.202302497](https://doi.org/10.1002/adma.202302497)
- 9 Chiu HS, Somvanshi S, Patel E, Chen TW, Singh VP, Zorman B, Patil SL, Pan Y, Chatterjee SS, Cancer Genome Atlas Research Network *et al.* (2018) Pan-cancer analysis of lncRNA regulation supports their targeting of cancer genes in each tumor context. *Cell Rep* **23**, 297–312.e12.
- 10 Shen-Orr SS, Milo R, Mangan S and Alon U (2002) Network motifs in the transcriptional regulation network of *Escherichia coli*. *Nat Genet* **31**, 64–68.
- 11 Cetin NS, Kuo CC, Ribarska T, Li R, Costa IG and Grummt I (2019) Isolation and genome-wide characterization of cellular DNA:RNA triplex structures. *Nucleic Acids Res* **47**, 2306–2321.
- 12 Maher LJ, Dervan PB and Wold B (1992) Analysis of promoter-specific repression by triple-helical DNA complexes in a eukaryotic cell-free transcription system. *Biochemistry* **31**, 70–81.
- 13 Mondal T, Subhash S, Vaid R, Enroth S, Uday S, Reinius B, Mitra S, Mohammed A, James AR, Hoberg E *et al.* (2015) MEG3 long noncoding RNA regulates the TGF- $\beta$  pathway genes through formation of RNA-DNA triplex structures. *Nat Commun* **6**, 1–17.
- 14 Kuo CC, Hänzelmann S, Sentürk Cetin N, Frank S, Zajzon B, Derks JP, Akhade VS, Ahuja G, Kanduri C, Grummt I *et al.* (2019) Detection of RNA-DNA binding sites in long noncoding RNAs. *Nucleic Acids Res* **47**, e32.
- 15 Cipolloni M, Fresch B, Occhiuto I, Rukin P, Komarova KG, Ceconello A, Willner I, Levine RD, Remacle F and Collini E (2017) Coherent electronic and nuclear dynamics in a rhodamine heterodimer-DNA supramolecular complex. *Phys Chem Chem Phys* **19**, 23043–23051.
- 16 Seeman NC and Sleiman HF (2017) DNA nanotechnology. *Nat Rev Mater* **3**, 1–23.
- 17 Kaufmann B, Willinger O, Kikuchi N, Navon N, Kermas L, Goldberg S and Amit R (2021) An oligo-library-based approach for mapping DNA-DNA triplex interactions in vitro. *ACS Synth Biol* **10**, 1808–1820.
- 18 Jenjaroenpun P, Chew CS, Yong TP, Choowongkamon K, Thammasorn W and Kuznetsov VA (2015) The TTSM database: a catalog of triplex target DNA sites associated with genes and regulatory elements in the human genome. *Nucleic Acids Res* **43**, D110–D116.
- 19 Pasquier C, Agnel S and Robichon A (2017) The mapping of predicted triplex DNA:RNA in the drosophila genome reveals a prominent location in development- and morphogenesis-related genes. *G3 (Bethesda)* **7**, 2295–2304.
- 20 Buske FA, Bauer DC, Mattick JS and Bailey TL (2012) Triplexator: detecting nucleic acid triple helices in genomic and transcriptomic data. *Genome Res* **22**, 1372–1381.
- 21 Filonov GS, Moon JD, Svensen N and Jaffrey SR (2014) Broccoli: rapid selection of an RNA mimic of green fluorescent protein by fluorescence-based selection and directed evolution. *J Am Chem Soc* **136**, 16299–16308.
- 22 Ouellet J (2016) RNA fluorescence with light-up aptamers. *Front Chem* **4**, 29.
- 23 Bouhedda F, Autour A and Ryckelynck M (2018) Light-up RNA aptamers and their cognate fluorogens: from their development to their applications. *Int J Mol Sci* **19**, 44.
- 24 Trachman RJ, Truong L and Ferré-D'Amaré AR (2017) Structural principles of fluorescent RNA aptamers. *Trends Pharmacol Sci* **38**, 928–939.
- 25 Ceconello A, Magro M, Vianello F and Simmel FC (2022) Rational design of hybrid DNA–RNA triplex structures as modulators of transcriptional activity in vitro. *Nucleic Acids Res* **1**, 13–14.
- 26 Milo R, Shen-Orr S, Itzkovitz S, Kashtan N, Chklovskii D and Alon U (2002) Network motifs: simple building blocks of complex networks. *Science* **298**, 824–827.
- 27 Elbaz J, Lioubashevski O, Wang F, Remacle F, Levine RD and Willner I (2010) DNA computing circuits using libraries of DNAzyme subunits. *Nat Nanotechnol* **5**, 417–422.
- 28 Seelig G, Soloveichik D, Zhang DY and Winfree E (2006) Enzyme-free nucleic acid logic circuits. *Science* **314**, 1585–1588.
- 29 Kunkler CN, Hulewicz JP, Hickman SC, Wang MC, McCown PJ and Brown JA (2019) Stability of an RNA•DNA–DNA triple helix depends on base triplet composition and length of the RNA third strand. *Nucleic Acids Res* **47**, 7213–7222.
- 30 Kotkowiak W, Kotkowiak M, Kierzek R and Pasternak A (2014) Unlocked nucleic acids: implications of increased conformational flexibility for RNA/DNA triplex formation. *Biochem J* **464**, 203–211.
- 31 Lilienthal S, Klein M, Orbach R, Willner I, Remacle F and Levine RD (2017) Continuous variables logic via coupled automata using a DNAzyme cascade with feedback. *Chem Sci* **8**, 2161–2168.
- 32 Borkotoky S, Meena CK, Bhalerao GM and Murali A (2017) An in-silico glimpse into the pH dependent structural changes of T7 RNA polymerase: a protein with simplicity. *Sci Rep* **7**, 1–12.
- 33 Rinn JL and Chang HY (2012) Genome regulation by long noncoding RNAs. *Annu Rev Biochem* **81**, 145–166.
- 34 Bao Z, Yang Z, Huang Z, Zhou Y, Cui Q and Dong D (2019) LncRNADisease 2.0: an updated database of long non-coding RNA-associated diseases. *Nucleic Acids Res* **47**, D1034–D1037.

- 35 Arora R, Brun CMC and Azzalin CM (2011) TERRA: long noncoding RNA at eukaryotic telomeres. *Prog Mol Subcell Biol* **51**, 65–94.
- 36 Adleman LM (1994) Molecular computation of solutions to combinatorial problems. *Science* **266**, 1021–1024.
- 37 Sancar G and Brunner M (2014) Circadian clocks and energy metabolism. *Cell Mol Life Sci* **71**, 2667–2680.
- 38 Brunner M and Schafmeier T (2006) Transcriptional and post-transcriptional regulation of the circadian clock of Cyanobacteria and *Neurospora*. *Genes Dev* **20**, 1061–1074.
- 39 Zhang J, Fakharzadeh A, Pan F, Roland C and Sagui C (2020) Atypical structures of GAA/TTC trinucleotide repeats underlying Friedreich's ataxia: DNA triplexes and RNA/DNA hybrids. *Nucleic Acids Res* **48**, 9899–9917.
- 40 Crook N, Ferreiro A, Condiotte Z and Dantas G (2020) Transcript barcoding illuminates the expression level of synthetic constructs in *E. coli* nissle residing in the mammalian gut. *ACS Synth Biol* **9**, 1010–1021.
- 41 Brophy JAN and Voigt CA (2014) Principles of genetic circuit design. *Nat Methods* **115**, 508–520.

## Supporting information

Additional supporting information may be found online in the Supporting Information section at the end of the article.

**Fig. S1.** Melting curve of 100 nM of TTS.

**Fig. S2.** Melting curves of 1  $\mu$ M TFO1 (black) and 10  $\mu$ M TFO2 (red).

**Table S1.** Nucleic acid sequences. DNA is black-colored, while RNA is blue-colored.